IEEE Robotics and Automation Letters (RA-L) paper, presented at ICRA 2026, Vienna, Austria. Cite as RA-L paper.

Stable Gravity Compensation and 6-DoF Manipulation of a Tethered Magnetic Endoscope With an Optimized End-Effector

Ahmed Hossameldin, Redwan Dahmouche, and Omar Tahri

***Abstract*—This paper presents the design and experimental validation of a magnetic end-effector optimized for the robust manipulation of a tethered magnetic endoscope in six-degrees-of-freedom (6-DoF). The symmetrical end-effector integrates two pairs of permanent magnets that generate a stable 2D attraction zone with a diameter exceeding 60 mm. This feature enables stable gravity compensation and precise control of centimeter-scale magnetic endoscopes. Experimental results demonstrate 6-DoF manipulation, stability and robustness against external disturbances, and successful navigation through obstacles in a confined environment. The stable gravity compensation allows to reduce friction and pressure on the endoscope's environment during navigation, which represent a key advantage for advancing minimally invasive medical procedures in general and colonoscopy in particular where minimizing pressure on the colon is critical. Future work will focus on enhancing the system through active control of the tether's length.**

***Index Terms*—Levitation and gravity compensation, medical robots and systems, telerobotics and teleoperation, 6-DoF magnetic robot, tethered endoscope.**

I. Introduction

MAGNETIC end-effectors are gaining increasing attention in medical robotics due to their ability to perform contactless manipulation and apply relatively high forces remotely over large distances [1], [2], [3]. In recent years, various magnetically actuated robots have been developed for multiple applications, including microrobot control [4], [5], catheter navigation [6], [7], and endoscope guidance [8], [9]. The magnetic field of the end-effector can be generated using either electromagnets or permanent magnets. Electromagnets offer the advantage of controllable magnetic field intensity; however, they require high electric currents to produce sufficiently strong magnetic fields, which can lead to heating and may necessitate cooling systems [10]. Moreover, electromagnets require complex feedback control systems for effective manipulation. Another drawback of electromagnetic end-effectors is their substantial size and weight compared to permanent magnets with equivalent magnetic moments, which limit their applications and reduce available workspace [11].

In contrast, permanent magnet end-effectors are valued for their ability to maintain strong magnetic fields in a compact form factor, without requiring external power sources or cooling systems. This makes them ideal for applications demanding high magnetic field strength [12], [13], [14]. Despite these advantages, stable control of manipulated magnetic objects is challenging, as it is physically impossible to create a point in 3D space that attracts magnetic objects from all directions [15]. One solution is to introduce feedback-controlled electromagnets, creating a hybrid system in which permanent magnets provide high forces and electromagnets stabilize the object [16]. However, this approach requires accurate pose measurement, which is particularly difficult in confined spaces typical of medical applications. An alternative method for achieving stable magnetic manipulation is to apply an external stabilizing force. This can come from gravity [17], [18], contact forces [19], surface tension [20], [21], [22], or a tether [17], [18], [23], either individually or in combination.

A promising concept for achieving stability without high-frequency feedback involves generating a stable region or point in 2D space where the magnetic field strength is locally maximal. A manipulated magnet is naturally attracted to this region, and the combination of magnetic forces, torques, and external forces maintains its equilibrium. As the manipulator moves or rotates, the magnetic object follows. Son et al. [24] applied this concept to develop a wireless millirobot navigation system within soft tissues using an array of permanent magnets. They created a stable magnetic trap zone that effectively attracted and stabilized the millirobot. However, the system was limited to 3-DoF, constraining movement and restricting the operational area. Moreover, the robot's stability was reliant on resistance from surrounding tissue—without such resistance, the system could not maintain stability.

Received 24 January 2025; accepted 30 May 2025. Date of publication 19 June 2025; date of current version 4 July 2025. This article was recommended for publication by Associate Editor K. Kim and Editor K.-U. Kyung upon evaluation of the reviewers' comments. This work was supported in part by EIPHI Graduate School under Contract ANR-17-EURE-0002, in part by Région Bourgogne Franche-Comté, in part by French RENATECH Network and its FEMTO-ST Technological Facility, in part by French ROBOTEX Network under Grant TIRREXANR-21-ESRE-0015 through FEMTO-ST Technological Facility CMNR, and in part by French ANR Project MiniSoRo under Grant ANR-19-CE10-0004. *(Corresponding author: Omar Tahri.)*

Ahmed Hossameldin is with Université de Bourgogne Europe, CNRS UMR 6303 ICB, F-21000 Dijon, France, and also with Université Marie et Louis Pasteur, SUPMICROTECH, CNRS, institut FEMTO-ST, F-25000 Besançon, France.

Redwan Dahmouche is with the Université Marie et Louis Pasteur, SUPMICROTECH, CNRS, institut FEMTO-ST, F-25000 Besançon, France (e-mail: redwan.dahmouche@femto-st.fr).

Omar Tahri is with the Université de Bourgogne Europe, CNRS UMR 6303 ICB, F-21000 Dijon, France, and also with the Saint Louis University, St. Louis, MO 63103 USA (e-mail: omar.tahri@ube.fr).

This article has supplementary downloadable material available at https://doi.org/10.1109/LRA.2025.3580971, provided by the authors.

Digital Object Identifier 10.1109/LRA.2025.3580971

In previous work, this principle was used to generate a 2D local maximum magnetic field ($2DLM$) for position control of a micromagnet on a liquid surface using a four-permanent-magnet end-effector [20]. In this setup, any magnetic particle within the attraction zone was drawn toward the $2DLM$, providing 2-DoF translational constraint via the magnetic field, while the third DoF was constrained by the liquid interface. This naturally stabilized the manipulated magnet's position without requiring feedback control. However, the system was limited to translational control with no demonstrated rotational control and was only capable of manipulating small magnetic particles.

In this paper, we introduce a four-magnet end-effector capable of stably compensating for gravity and manipulating a tethered magnetic endoscope, enabled by its wide attraction zone and strong magnetic forces. These magnetic forces allow for both disturbance rejection and gravity compensation, while the large attraction zone facilitates the manipulation of larger magnetic bodies. In combination with the tension provided by a fixed-length tether, the end-effector enables natural stabilization and independent control of 3-DoF in translation and 3-DoF in rotation. This development opens up new possibilities for industrial and medical applications, including minimally invasive procedures such as colonoscopy.

II. Modeling and Background

In designing a multi-magnet end-effector, it is essential to derive the equations that govern magnetic fields, forces, and torques for interacting magnets. A fundamental property of quasi-static magnetic flux, $\mathbf{B}$, is that it does not allow magnetic sources or sinks. This can be mathematically expressed as:

$$\nabla \cdot \mathbf{B} = 0, \tag{1}$$

where $\nabla\cdot$ denotes the divergence operator. The magnetic force $\mathbf{F}_\mathrm{B}$ exerted on a magnetic object depends on its magnetic moment $\mathbf{M}$ and the external magnetic flux density $\mathbf{B}$:

$$\mathbf{F}_\mathrm{B} = \nabla(\mathbf{M} \cdot \mathbf{B}), \tag{2}$$

where ∇ and $\cdot$ represent the gradient and dot product operators, respectively.

Since the magnetic dipole moment of a permanent magnet is constant, the above equation can be rewritten as:

$$\mathbf{F}_\mathrm{B} = \begin{pmatrix} F_{B_x} \\ F_{B_y} \\ F_{B_z} \end{pmatrix} = \begin{pmatrix} \frac{\partial B_x}{\partial x} & \frac{\partial B_y}{\partial x} & \frac{\partial B_z}{\partial x} \\ \frac{\partial B_x}{\partial y} & \frac{\partial B_y}{\partial y} & \frac{\partial B_z}{\partial y} \\ \frac{\partial B_x}{\partial z} & \frac{\partial B_y}{\partial z} & \frac{\partial B_z}{\partial z} \end{pmatrix} \begin{pmatrix} M_x \\ M_y \\ M_z \end{pmatrix}. \tag{3}$$

This equation shows that the resulting magnetic force is directly proportional to the gradient of the magnetic field and the magnetic moment of the permanent magnet [25]. For a given magnet, increasing the force requires enhancing the magnetic field gradient at the magnet's location.

In addition, a magnet subjected to an external magnetic field experiences a torque, $\boldsymbol{\tau}_\mathrm{B}$, which tends to align the magnetic dipole moment with the field:

$$\boldsymbol{\tau}_\mathrm{B} = \mathbf{M} \times \mathbf{B}, \tag{4}$$

where $\times$ denotes the cross product.

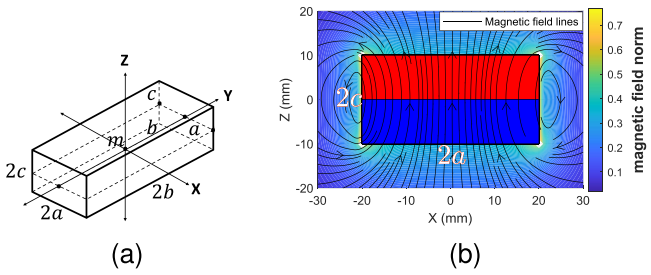

Fig. 1. (a) Rectangular prism permanent magnet schematic. (b) The X-Z plane of the rectangular permanent magnet, showing the magnetic field norm in Tesla and magnetic field lines.

Pure rotation of a magnetic dipole about its own magnetic moment does not affect the force or torque. Therefore, up to 5-DoF can be controlled for magnetic dipoles using magnetic forces and torques [26].

The components of the magnetic field, B_x, B_y, and B_z, generated by a rectangular permanent magnet magnetized along the Z-axis can be analytically described using the model proposed by Camacho et al. [27]:

$$B_x = \frac{\mu_0 M}{4\pi} \ln \frac{k_2(-x,y,-z)k_2(x,y,z)}{k_2(x,y,-z)k_2(-x,y,z)}, \tag{5}$$

$$B_y = \frac{\mu_0 M}{4\pi} \ln \frac{k_2(-y,x,-z)k_2(y,x,z)}{k_2(y,x,-z)k_2(-y,x,z)}, \tag{6}$$

$$\begin{aligned} B_z = & -\frac{\mu_0 M}{4\pi} [k_1(-x,y,z) + k_1(-x,y,-z) \\ & + k_1(-x,-y,z) + k_1(-x,-y,-z) + k_1(x,y,z) \\ & + k_1(x,y,-z) + k_1(x,-y,z) + k_1(x,-y,-z)]. \end{aligned} \tag{7}$$

Here, μ_0 is the permeability of free space, and a, b, and c represent the magnet's dimensions, as illustrated in Fig. 1. The coordinates x, y, and z refer to the points where the magnetic field is evaluated, relative to the magnet's origin.

The coefficients k_1 and k_2 are defined as:

$$\begin{aligned} k_1(x,y,z) &= \arctan \frac{(x+a)(y+b)}{(z+c)\sqrt{(x+a)^2+(y+b)^2+(z+c)^2}}, \\ k_2(x,y,z) &= \frac{\sqrt{(x+a)^2+(y-b)^2+(z+c)^2}+b-y}{\sqrt{(x+a)^2+(y+b)^2+(z+c)^2}-b-y}. \end{aligned} \tag{8}$$

III. Design and Optimization of a Tethered Permanent-Magnet Endoscope

A. Modeling of the Tethered Magnetic Endoscope

During operation, endoscopes are typically connected to the exterior of the body for real-time navigation and the transfer of energy and data. This architecture also facilitates the extraction of the endoscope in case of malfunction. Since the patient's primary discomfort arises from pressure exerted by the endoscopic head on the colon during insertion, magnetic endoscopes aim to reduce this pressure by pulling the device using magnetic forces.

The conventional approach involves varying the position and, if applicable, the magnetization of the electromagnetic end-effector to control the endoscope's position [28] (see Fig. 2(a)). However, this position is inherently unstable, as a magnetic

IEEE Robotics and Automation Letters (RA-L) paper, presented at ICRA 2026, Vienna, Austria. Cite as RA-L paper.

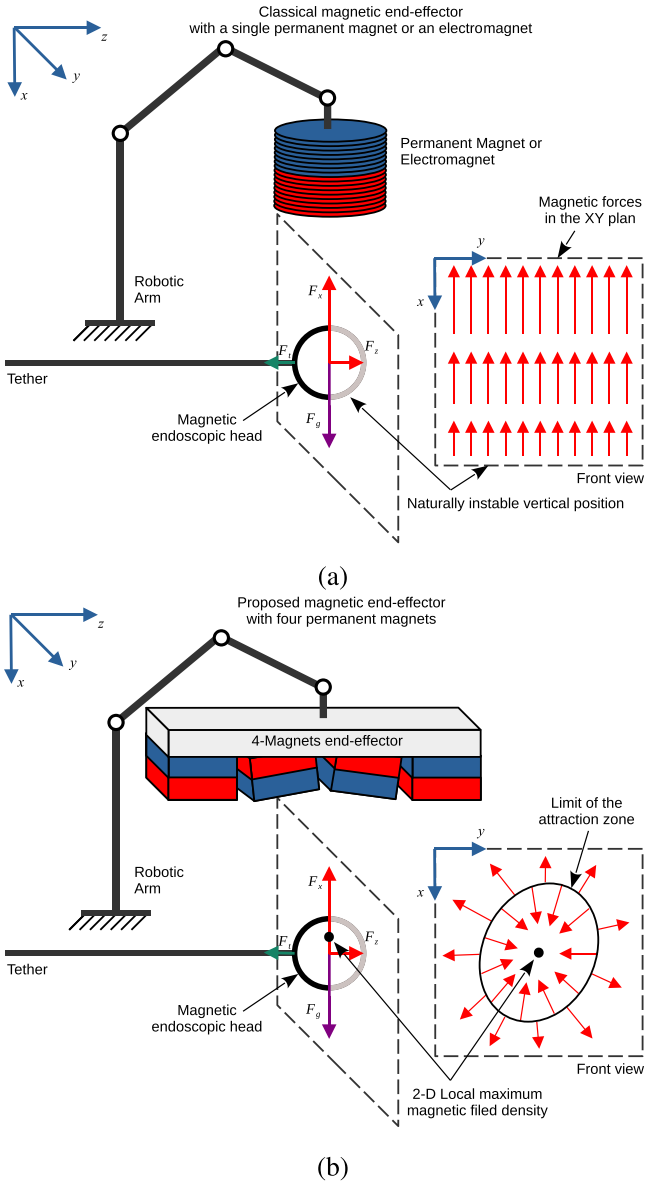

Fig. 2. Originality of the proposed concept. (a) Conventional approach with a single magnet: vertical position is unstable because the magnetic force increases as the endoscope approaches the end-effector. (b) Proposed concept: the endoscope is stabilized in the XY plane by a magnetic field that draws it toward a local maximum. This magnetic force counteracts gravity and disturbances.

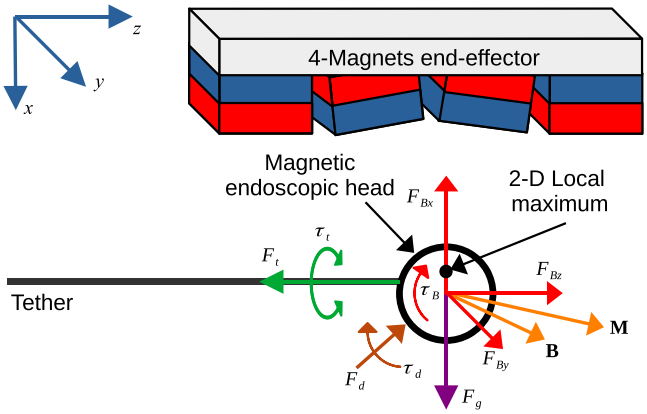

Fig. 3. System of forces and torques acting on the magnetic endoscope. $\mathbf{F}_B$ the force and τ_B torque applied by the magnetic end-effector, $\mathbf{F_t}$ the force and τ_t torque applied by the tether, the disturbing forces $\mathbf{F}_d$ and torques $\boldsymbol{\tau}_d$, and the gravity force $\mathbf{F}_g$.

dipole cannot be stabilized using only static permanent magnets. Although generating a true magnetic field maximum in 3D space is theoretically impossible, creating a local maximum in 2D is feasible. The magnetic end-effector constrains two DoF in both rotation and translation via this 2D local maximum. The remaining rotational DoF is stabilized by the tether, while the final translational DoF is constrained by the opposing forces of the magnet and tether. Consequently, all DoF of the magnetic capsule can be controlled.

The tether used in this study is a standard flexible endoscopic camera cable, which offers the desirable properties of high bending compliance and high torsional rigidity. These characteristics allow the tether to accommodate the capsule's motion while minimizing unwanted twisting. Its torsional stiffness also generates shear forces during rotation, assisting the capsule in self-aligning. Any relative positioning errors can be corrected using the end-effector's 3-DoF translational capabilities, ensuring precise and robust control.

The most critical aspect of the design is generating a 2D local maximum in the magnetic field that can attract and levitate the magnetic endoscopic head. This strategy, referred to as magnetic gravity compensation, relies solely on magnetic forces in the vertical direction, as illustrated in Fig. 2(b). An important characteristic of this approach is that the maximum vertical force—required to counteract gravity—occurs at the symmetry plane, while the tether force along the z-axis is minimal at this location. This configuration maximizes vertical support while minimizing friction from the tether, which is particularly beneficial for colonoscopy applications.

To realize this behavior, the magnetic end-effector must be carefully designed and optimized to generate a strong 2D magnetic field maximum with a wide attraction zone—defined as the region in which any magnetic object is drawn toward the maximum. This can be achieved using two symmetrical pairs of magnets, as shown in Fig. 4.

The system of forces and torques acting on the magnetic endoscope is illustrated in Fig. 3. The magnetic end-effector applies a force $\mathbf{F}_B$. The F_{B_x} and F_{B_y} components of $\mathbf{F}_B$ attract the endoscope toward the 2D local maximum in the XY plane, while F_{B_z} pushes it away from the symmetry plane. Because the planar position is naturally stable, only the Z direction requires active stabilization, which is provided by the tether applying a tension force F_t. If the sum of the magnetic, the gravitational, and the disturbance forces is not colinear with F_t then a torque is required to counteract the resulting moment. This is provided by the magnetic torque $\boldsymbol{\tau}_B$, which tries to align the magnetic moment $\mathbf{M}$ of the endoscope with the magnetic field $\mathbf{B}$. It is important to note that no magnetic torque is applied about the endoscope's magnetic moment itself; this torque is constrained only by the torsional stiffness of the tether. While controlling rotation around the magnetic moment is not strictly necessary,

IEEE Robotics and Automation Letters (RA-L) paper, presented at ICRA 2026, Vienna, Austria. Cite as RA-L paper.

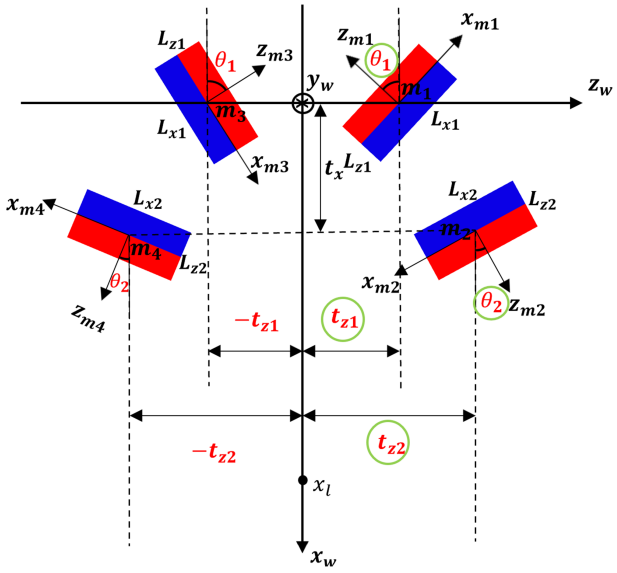

Fig. 4. Design of the four-magnet end-effector. Four variables (t_{z_1}, t_{z_2}, θ_1, θ_2) are optimized to generate a 2D local maximum (2DLM) at $(x_l, 0, 0)$.

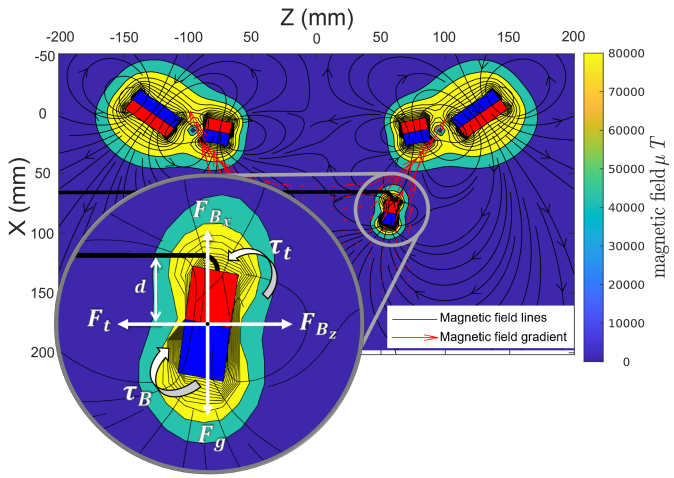

Fig. 5. Tethered cylindrical magnetic endoscope levitated by the four-magnet end-effector. Contours represent magnetic flux density; black lines show magnetic field lines, and red arrows indicate the gradient. The magnetic torque on the capsule depends on field strength and orientation relative to the capsule's magnetic moment. The magnetic force is proportional to the field gradient. By adjusting end-effector orientation, different equilibrium points can be achieved.

full 6-DoF control is achieved by simultaneously adjusting the position and orientation of both the magnetic end-effector and the tether. The system remains in equilibrium as long as disturbing forces $\mathbf{F}_d$, torques $\boldsymbol{\tau}_d$, and gravity $\mathbf{F}_g$ are counteracted by magnetic forces. The system's performance depends on the characteristics of both the magnetic end-effector and the tether: the former should exhibit a large attraction zone and strong field gradient, and the latter should be flexible yet torsionally rigid.

The final design features a four-magnet end-effector with two symmetry planes at $y = 0$ and $z = 0$. In the end-effector's reference frame, the magnet centers are located at $p_1(0, 0, t_{z_1})$, $p_2(t_x, 0, t_{z_2})$, $p_3(0, 0, -t_{z_1})$, and $p_4(t_x, 0, -t_{z_2})$. The parameter t_x was fixed at 15 mm based on preliminary studies showing limited influence on optimization outcomes. All magnetic moments lie in the X-Z plane, with respective orientations of θ_1, θ_2, $-\theta_1$, and $-\theta_2$, as shown in Fig. 4.

The resulting magnetic field was obtained by applying each magnet's translation and orientation, then superimposing their fields. Due to the end-effector's symmetry, the resulting field has specific properties: B_x is even, B_y is odd, and B_z is zero in the $Z = 0$ plane. Fig. 5 shows the magnetic field norm, lines and gradient.

B. Optimization of the Magnetic End-Effector

The optimization goal was to design a four-magnet end-effector that produces strong magnetic forces and torques, as well as a broad attraction zone. Based on (3), magnetic force is maximized when the magnet aligns with the external field. However, increasing the magnetic moment $\mathbf{M}$ also increases magnet volume and weight, which is undesirable. Therefore, improving the magnetic field gradient is a more practical strategy for effective gravity compensation.

Optimization targeted the parameters t_{z_1}, t_{z_2}, θ_1, θ_2, and magnet dimensions L_{x_2}, L_{y_2}, and L_{z_2} to maximize the field gradient at a desired point. The local maximum was constrained to the X-axis due to symmetry, where $\sum B_y = \sum B_z = 0$, simplifying analysis. The x-component, $\sum B_x$, was used to locate the maximum. Unless otherwise noted, all parameters refer to the entire end-effector.

Conditions for a local maximum at $(x_l, 0, 0)$ include:

a) $\frac{\partial B_x}{\partial x} = 0$ (first derivative zero),

b) $\frac{\partial^2 B_x}{\partial x^2} < 0$ (concavity for maximum),

c) $\frac{\partial^2 B_n}{\partial x^2}\frac{\partial^2 B_n}{\partial y^2} - (\frac{\partial^2 B_n}{\partial x \partial y})^2 > 0$ (avoid saddle points),

d) No physical collisions between magnets.

Optimization was conducted in two stages: identifying admissible solutions and maximizing the magnetic field norm and attraction zone at the desired local maximum. The implementation was done in MATLAB 2024a and executed on a DELL Precision 3561 with 32 GB RAM and an 11th Gen Intel Core$^{\text{TM}}$i9-11950H @ 2.60 GHz $\times$ 16 processor. The full optimization converged in approximately 3 hours, yielding the optimal configuration parameters.

IV. Simulations and Experimental Results

A. Optimized Magnetic End-Effector

Given the constraints and the objective function, we optimized the design of the end-effector to maximize the magnetic field density at the point on the x-axis, $x_l = 80$ mm. For the optimization, the admissible translation and rotation parameters were constrained $10 < t_{z_{1,2}} < 130$ mm and $0^\circ < \theta_{1,2} < 180^\circ$, respectively. The outer magnet dimensions were limited to $5\,\text{mm} < L_{x_2, y_2, z_2} < 40\,\text{mm}$. The value of t_x was set to 15 mm, and the diameter of the attraction zone was at least 60 mm around the local maximum.

The optimized parameters of the magnetic end-effector are presented in Table I (see Fig. 4 for reference).

IEEE Robotics and Automation Letters (RA-L) paper, presented at ICRA 2026, Vienna, Austria. Cite as RA-L paper.

TABLE I
OPTIMIZED DESIGN PARAMETERS OF THE END-EFFECTOR

Parameter	Value	Parameter	Value
L_{x_1} (mm)	40	L_{z_2} (mm)	20
L_{x_2} (mm)	20	t_{z_1} (mm)	126.5
L_{y_1} (mm)	40	t_{z_2} (mm)	77
L_{y_2} (mm)	20	θ_1°	53.5
L_{z_1} (mm)	20	θ_2°	78.12

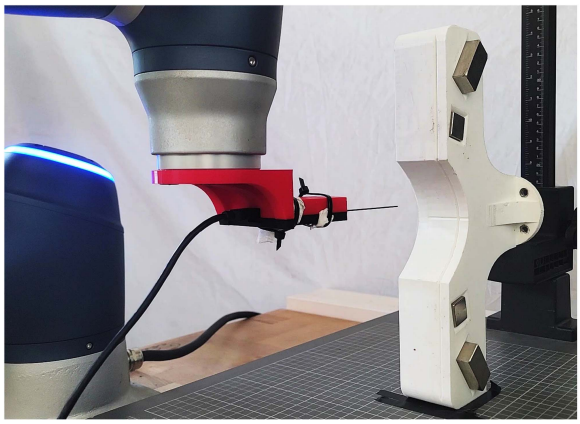

Fig. 6. Experimental setup for measuring the magnetic field using a 3MTS USB Teslameter and a Doosan A0509 s robotic arm.

B. Simulation and Validation of the Optimized End-Effector's Magnetic Field

To validate the generated magnetic field, the optimized end-effector was 3D-printed, and Neodymium N45 magnets were used. Magnetic field components along the three axes were measured using a Senis 3MTS USB Teslameter mounted on a Doosan A0509 s robotic arm. During the experiment, the magnetic end-effector remained stationary while the Teslameter was precisely positioned in the XY plane by the robotic arm. At each measurement point, the robotic arm halted, and 100 static magnetic field measurements were recorded at small time intervals. The averaged values were used to reduce noise and ensure accuracy. This process was repeated systematically to cover the entire target area. Fig. 6 shows the experimental setup.

Fig. 7 illustrates the simulated and experimentally measured magnetic field densities in the XY plane at various z-positions. The left column shows theoretical results, while the right column shows experimental measurements. Both magnetic field distributions exhibit similar shapes, with local maxima appearing at approximately the same location. As expected, the attraction zone is broad at $z = 0$, narrowing as z increases, and eventually disappears. Although the local maximum is located at $x_l = 80$ mm on the plane $z = 0$ as optimized, its location varies for different z values, forming a 3D attraction zone shape more closely resembling a croissant than a sphere.

C. Tethered Gravity Compensation and Manipulation of a Magnetic Endoscope

We evaluated the optimized end-effector for tethered gravity compensation and manipulation using two types of magnetic

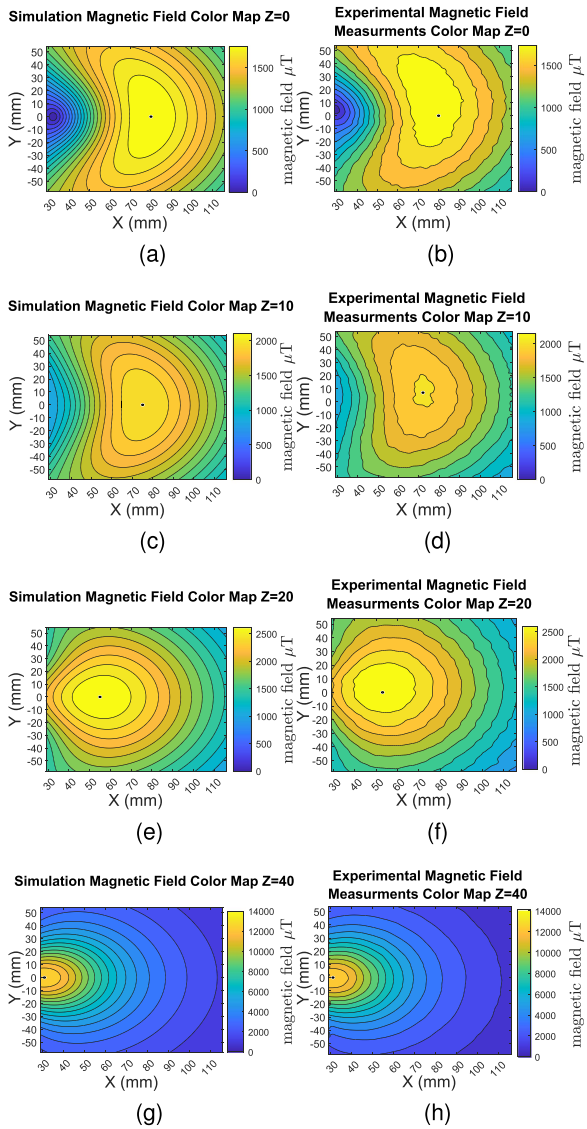

Fig. 7. Simulated and experimentally measured magnetic field norms at different z-axis planes. A 2D local maximum is clearly observable, validating the optimization.

endoscopes: one spherical and one cylindrical. Each was equipped with a wired camera and an N45 neodymium magnet. The magnetic end-effector, mounted on a Doosan A0509 s robotic arm, performed 6-DoF motion. The camera detected a pattern to estimate the 6-DoF pose of the endoscope, which was tethered to the end-effector. The tether was used both for real-time image transmission and to enhance Z-axis stabilization.

The first experiment assessed the stability of the gravity compensation and its robustness against disturbances. Each was placed inside the attraction zone and manual disturbances of more than 40 mm were applied (see Fig. 8). Fig. 9 shows the endoscopes' displacements over time. The cylindrical design reached a maximum of 55 mm and the spherical 43.1 mm. Both recovered and re-stabilized after oscillations, confirming robustness. The measured stable zone is adequate for colonoscopy, given average colon diameters [29].

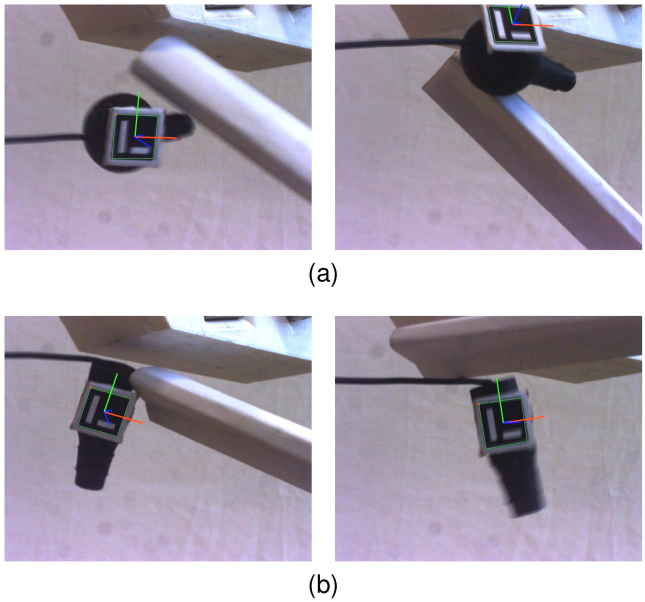

Fig. 8. Gravity compensation robustness against external disturbances of different tethered endoscope shapes: (a) spherical, (b) cylindrical.

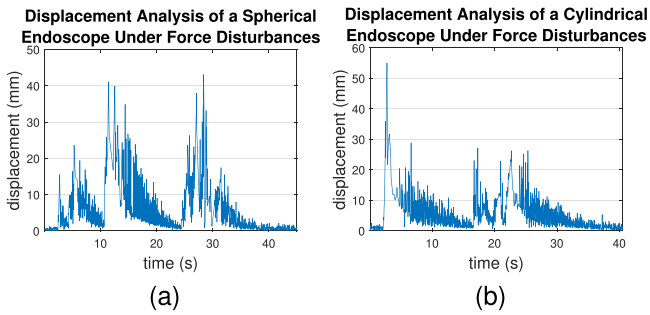

Fig. 9. Displacement of (a) spherical and (b) cylindrical endoscopes after disturbance.

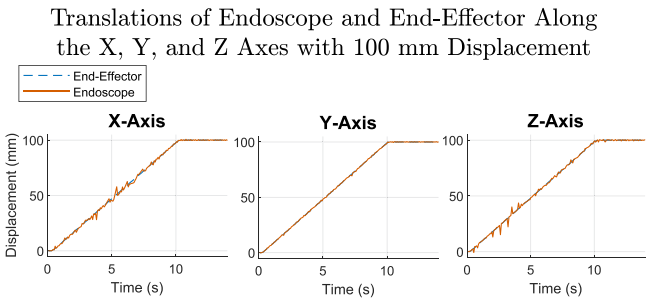

Fig. 10. Tracking accuracy during 100-mm translations along the X-, Y-, and Z axes.

In the second experiment, the magnetic end-effector performed independent 100 mm translations along the X-, Y-, and Z-axes. The endoscope's position was measured using visual markers. As shown in Fig. 10, the endoscope tracked the end-effector's motion with minor oscillations due to acceleration and deceleration.

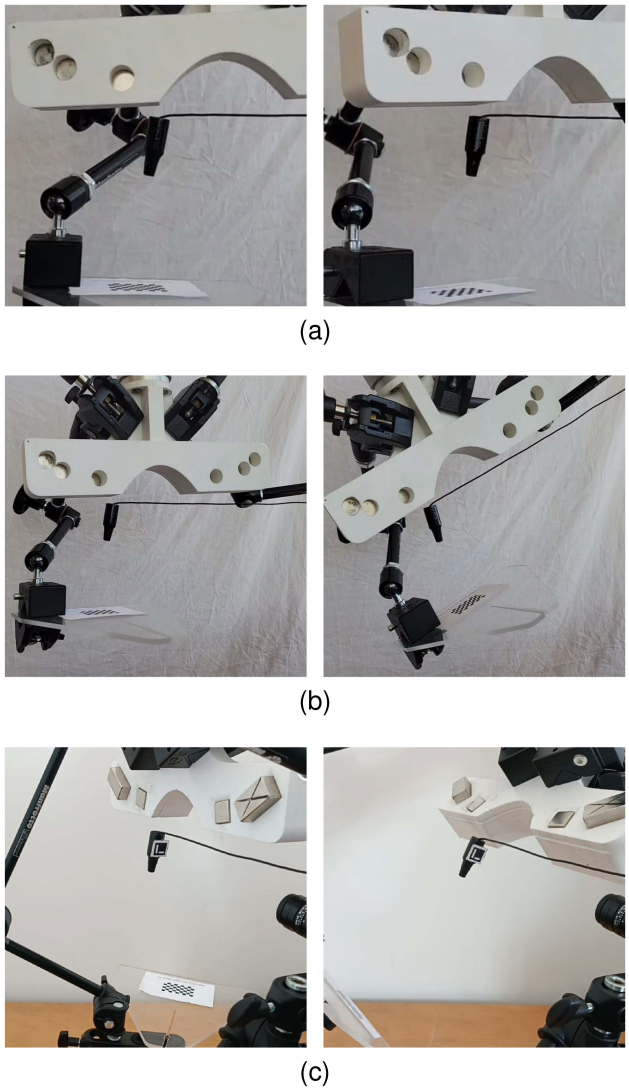

Fig. 11. Rotation experiment of the weight-compensated tethered endoscope: (a) X-axis, (b) Y-axis, (c) Z-axis.

Next, the end-effector performed rotations about the X-, Y-, and Z-axes. While the endoscope accurately tracked the rotations of the magnetic end-effector about the X-and Y-axes from 0 to 30°, a consistent rotation ratio of approximately 0.486 was observed between the end-effector and endoscope during Z-axis rotations. To compensate for this discrepancy, a fixed open-loop gain of 2.05 was implemented. As a result, achieving a 25° rotation of the endoscope requires a 51.4° rotation of the end-effector. Figs. 11 and 12 illustrate the repeated corresponding rotation motion of the cylindrical magnetic endoscope. Although the Z-axis rotation is more prone to oscillations, the endoscope closely followed the desired trajectory. The errors between the desired and the obtained translation and rotation trajectories are illustrated in Fig. 13.

To assess the precision of the magnetic endoscope, a comprehensive statistical analysis of trajectory errors was conducted across repeated trials. Table II presents key metrics for both translational and rotational errors. For translations, standard

IEEE Robotics and Automation Letters (RA-L) paper, presented at ICRA 2026, Vienna, Austria. Cite as RA-L paper.

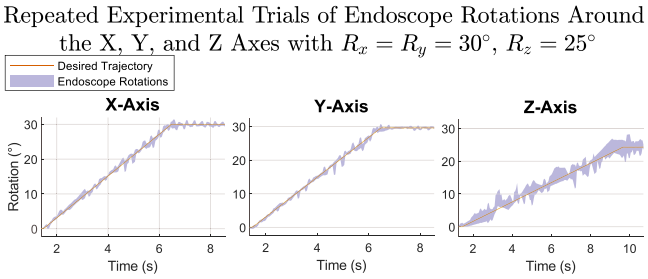

Fig. 12. Rotational motion of the weight-compensated magnetic endoscope of repeated experiments for $R_x = R_y = 30°$ and $R_z = 25°$ rotations.

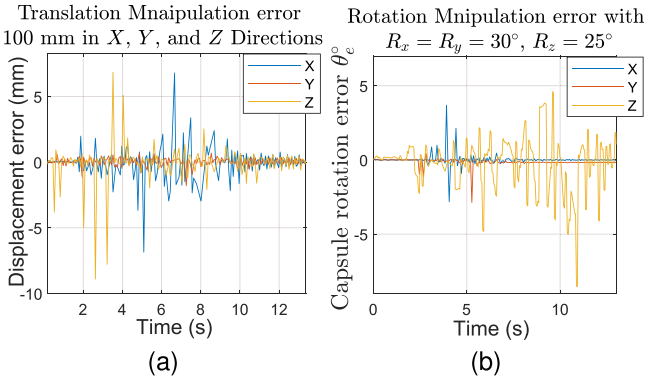

Fig. 13. 6-DoF experimental manipulation error analysis: (a) Translation errors along the X-, Y-, and Z -axes during 100mm displacements of the end-effector and capsule. Errors were calculated by estimating the pose of a reference pattern via the capsule camera and measuring deviations from the target positions. (b) Rotation errors around the X-, Y-, and Z-axes for end-effector rotations of $30°$ (X, Y) and $51.4°$ (Z), and capsule rotations of $30°$ (X, Y) and $25°$ (Z). Errors were computed by comparing the target rotation angles with the measured capsule rotations using pattern-based pose estimation.

TABLE II
6-DoF Manipulation Error Analysis

Metric	Axis	Std. Dev.	Mean Error	Max Error
Translation (mm)	X	1.1897	-0.0256	6.7
	Y	0.2827	0.0332	1.7
	Z	0.6732	-0.0845	8.9
Rotation (°)	X	0.2113	0.0148	3.6
	Y	0.2113	-0.1414	2.8
	Z	1.5901	-0.2601	8.5

deviations ranged from 0.28 mm (Y-axis) to 1.19 mm (X-axis), with maximum errors reaching 8.9 mm (Z-axis). Rotational analysis showed standard deviations between 0.21° (X- and Y-axes) and 1.59° (Z-axis), with peak errors of 8.5° on the Z-axis. These results highlight the system's precision and reliability, with the Z-axis exhibiting the greatest variability in both translational and rotational measurements.

To evaluate the endoscope's ability to navigate between obstacles, another experiment was conducted using telemanipulation of the weight-compensated magnetic endoscope from an initial position to a target location, as shown in Fig. 14. The

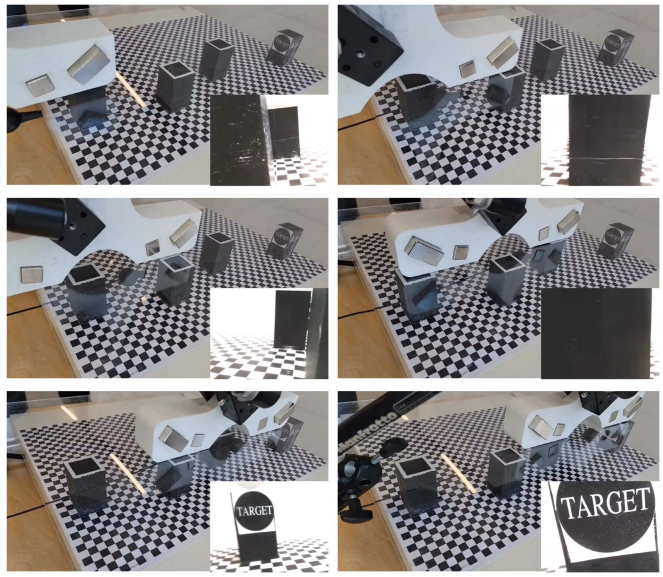

Fig. 14. Open-loop telemanipulation of the weight-compensated endoscope demonstrating obstacle avoidance from initial to target position.

endoscope successfully navigated through obstacles to reach the destination. These results demonstrate the system's ability to manipulate the weight-compensated endoscope along curved trajectories. A video accompanying this paper further illustrates the robotized magnetic endoscope's capabilities.

V. Discussion

The experimental results confirm the effectiveness of the proposed magnetic end-effector in achieving stable weight compensation and full 6-DoF control of a tethered magnetic endoscope. The system consistently maintained the endoscope's position within a stable two-dimensional attraction zone generated by the optimized magnetic field. This stability was preserved even under significant external disturbances exceeding 40 mm, demonstrating strong robustness.

A key outcome of this work was the ability to navigate the magnetic endoscope through constrained environments without exerting pressure on surrounding surfaces. This was achieved by maintaining a magnetic equilibrium zone that minimized interaction forces with the anatomical environment—a critical feature for procedures such as colonoscopy. Experimental demonstrations confirmed that the endoscope could move smoothly between obstacles, guided solely by the magnetic end-effector and the tether.

Despite these encouraging results, several areas for improvement remain before clinical deployment. One primary limitation is that the stability of the magnetic endoscope depends on its relative position with respect to the end-effector. Currently, the tether is fixed in length and attached directly to the end-effector, which limits its ability to accommodate complex anatomical geometries. Navigating curved segments of the colon may displace the endoscope outside the attraction zone, potentially affecting stability and performance.

To address this limitation, future versions of the system should incorporate active tether-length control. A promising approach would involve real-time tension sensing in the tether to dynamically adjust its length. This strategy would also enable regulation of the pressure exerted by the tether on the intestinal walls. Minimizing this pressure is essential to reduce patient discomfort and avoid complications. While reducing the tether's diameter may seem beneficial, a more suitable approach is to maintain a minimal yet adequate diameter that ensures pressure is distributed effectively, while combining high bending flexibility with significant torsional rigidity. The size of the endoscope and tether diameter can be optimized for greater patient comfort.

Another design consideration involves rotational control around the endoscope's magnetic moment. Although active control of this axis is not required for routine inspection and navigation, it can still be achieved by employing a tether with sufficient torsional stiffness. Enabling this control would expand the system's capabilities in scenarios that demand full 6-DoF actuation, such as targeted biopsies or therapeutic interventions.

VI. Conclusion

In this paper, we presented a novel 6-DoF robotized, magnetically actuated tethered endoscopic system. The system comprises a four-permanent-magnet end-effector mounted on a 7-DoF robotic arm and a tethered magnetic endoscope. The proposed design effectively and robustly compensates for the endoscope's weight, maintaining stability even under disturbances exceeding 40 mm. Experimental results demonstrated that the magnetic endoscope can be controlled across all 6-DoF and navigate through confined spaces with obstacles while minimizing the pressure exerted on its surroundings. These promising outcomes lay the foundation for future applications in minimally invasive colonoscopy. The compact size of the endoscope and tether was considered to enhance patient comfort.

A current limitation of the system is the fixed tether length, which restricts adaptability in navigating long or highly curved anatomical pathways. In future work, we aim to implement active tether-length control to enhance the system's versatility and performance.

Acknowledgment

The experiments presented in this paper were conducted using the materials and facilities available at the CNRS UMR 6303 ICB laboratory in Dijon, France.

References

[1] Z. Chen et al., "A magnetic multi-layer soft robot for on-demand targeted adhesion," *Nature Commun.*, vol. 15, no. 1, 2024, Art. no. 644.

[2] Y. Xiang et al., "MINRob: A large force-outputting miniature robot based on a triple-magnet system," *IEEE Trans. Robot.*, vol. 40, pp. 3127–3145, 2024.

[3] Z. Yang, H. Yang, Y. Cao, Y. Cui, and L. Zhang, "Magnetically actuated continuum medical robots: A review," *Adv. Intell. Syst.*, vol. 5, no. 6, p. 2200416, 2023.

[4] L. Yang and L. Zhang, "Motion control in magnetic microrobotics: From individual and multiple robots to swarms," *Annu. Rev. Control Robot., Auton. Syst.*, vol. 4, pp. 509–534, 2021.

[5] B. Ahmad, M. Gauthier, G. J. Laurent, and A. Bolopion, "Mobile microrobots for in vitro biomedical applications: A survey," *IEEE Trans. Robot.*, vol. 38, no. 1, pp. 646–663, Feb. 2022.

[6] J. Hwang, J.-Y. Kim, and H. Choi, "A review of magnetic actuation systems and magnetically actuated guidewire-and catheter-based microrobots for vascular interventions," *Intell. Service Robot.*, vol. 13, pp. 1–14, 2020.

[7] C. Limpabandhu, Y. Hu, H. Ren, W. Song, and Z. T. Ho Tse, "Magnetically steerable catheters: State of the art review," *Proc. Inst. Mech. Engineers, Part H: J. Eng. Med.*, vol. 237, no. 3, pp. 297–308, 2023.

[8] A. Alian et al., "Current engineering developments for robotic systems in flexible endoscopy," *Techn. Innov. Gastrointestinal Endoscopy*, vol. 25, no. 1, pp. 67–81, 2023.

[9] W. Chen, J. Sui, and C. Wang, "Magnetically actuated capsule robots: A review," *IEEE Access*, vol. 10, pp. 88398–88420, 2022.

[10] F. Ongaro, S. Pane, S. Scheggi, and S. Misra, "Design of an electromagnetic setup for independent three-dimensional control of pairs of identical and nonidentical microrobots," *IEEE Trans. Robot.*, vol. 35, no. 1, pp. 174–183, Feb. 2019.

[11] A. J. Petruska, J. B. Brink, and J. J. Abbott, "First demonstration of a modular and reconfigurable magnetic-manipulation system," in *Proc. IEEE Int. Conf. Robot. Automat.*, 2015, pp. 149–155.

[12] J. J. Abbott, E. Diller, and A. J. Petruska, "Magnetic methods in robotics," *Annu. Rev. Control, Robot., Auton. Syst.*, vol. 3, pp. 57–90, 2020.

[13] P. Ryan and E. Diller, "Magnetic actuation for full dexterity microrobotic control using rotating permanent magnets," *IEEE Trans. Robot.*, vol. 33, no. 6, pp. 1398–1409, Dec. 2017.

[14] Z. Yang and L. Zhang, "Magnetic actuation systems for miniature robots: A review," *Adv. Intell. Syst.*, vol. 2, no. 9, 2020, Art. no. 2000082.

[15] A. J. Petruska and B. J. Nelson, "Minimum bounds on the number of electromagnets required for remote magnetic manipulation," *IEEE Trans. Robot.*, vol. 31, no. 3, pp. 714–722, Jun. 2015.

[16] A. Z. Taddese, P. R. Slawinski, M. Pirotta, E. De Momi, K. L. Obstein, and P. Valdastri, "Enhanced real-time pose estimation for closed-loop robotic manipulation of magnetically actuated capsule endoscopes," *Int. J. Robot. Res.*, vol. 37, no. 8, pp. 890–911, 2018.

[17] G. Pittiglio et al., "Magnetic levitation for soft-tethered capsule colonoscopy actuated with a single permanent magnet: A dynamic control approach," *IEEE Robot. Automat. Lett.*, vol. 4, no. 2, pp. 1224–1231, Apr. 2019.

[18] G. Pittiglio, J. H. Chandler, M. Richter, V. K. Venkiteswaran, S. Misra, and P. Valdastri, "Dual-arm control for enhanced magnetic manipulation," in *Proc. IEEE/RSJ Int. Conf. Intell. Robots Syst.*, 2020, pp. 7211–7218.

[19] A. W. Mahoney and J. J. Abbott, "Generating rotating magnetic fields with a single permanent magnet for propulsion of untethered magnetic devices in a lumen," *IEEE Trans. Robot.*, vol. 30, no. 2, pp. 411–420, Apr. 2014.

[20] A. Zarrouk, K. Belharet, O. Tahri, and A. Ferreira, "A four-magnet system for 2D wireless open-loop control of microrobots," in *Proc. Int. Conf. Robot. Automat.*, 2019, pp. 883–888.

[21] W. Amokrane, K. Belharet, M. Souissi, A. B. Grayeli, and A. Ferreira, "Macro–micromanipulation platform for inner ear drug delivery," *Robot. Auton. Syst.*, vol. 107, pp. 10–19, 2018.

[22] T. Petit, L. Zhang, K. E. Peyer, B. E. Kratochvil, and B. J. Nelson, "Selective trapping and manipulation of microscale objects using mobile microvortices," *Nano Lett.*, vol. 12, no. 1, pp. 156–160, 2012.

[23] A. Z. Taddese, P. R. Slawinski, K. L. Obstein, and P. Valdastri, "Closed loop control of a tethered magnetic capsule endoscope," *Robot. Sci. Syst.: Online Proc.*, vol. 2016, pp. 10–15 607, 2016, doi: 10.15607/RSS.2016.XII.018.

[24] D. Son, M. C. Ugurlu, and M. Sitti, "Permanent magnet array–driven navigation of wireless millirobots inside soft tissues," *Sci. Adv.*, vol. 7, no. 43, 2021, Art. no. eabi8932.

[25] R. E. Cohen, D. Lide, and G. Trigg, *Physicist's Desk Reference*. Berlin, Germany: Springer, 2003.

[26] S. Yuan, Y. Wan, and S. Song, "RectMag3D: A magnetic actuation system for steering milli/microrobots based on rectangular electromagnetic coils," *Appl. Sci.*, vol. 10, no. 8, 2020, Art. no. 2677.

[27] J. M. Camacho and V. Sosa, "Alternative method to calculate the magnetic field of permanent magnets with azimuthal symmetry," *Revista Mex. de física E*, vol. 59, no. 1, pp. 8–17, 2013.

[28] C. A. Landewee et al., "Magnetic flexible endoscope: A novel platform for diagnostic and therapeutic colonoscopy," *iGIE*, vol. 3, no. 1, pp. 1–4, 2024.

[29] F. P. Rossini and V. Cameron-Curry, *Atlas of Coloscopy*. Berlin, Germany: Springer, 1975.